Superhydrophobic sodium alginate/cellulose aerogel for the dye adsorption and oil-water separation

Huimin Li
Jiangnan University
Jingyi Huang
Jiangnan University
Chaoran Meng
Jiangnan University
Shen Shen
Jiangnan University
Hongbo Wang
Jiangnan University
Jiajia Fu (kathyfjj@126.com)
Jiangnan University

Research Article

Keywords: Polysaccharide-based aerogel, Hydrophobicity, Dye adsorption, Oil-water separation

Posted Date: October 13th, 2022

DOI: https://doi.org/10.21203/rs.3.rs-2134219/v1

Superhydrophobic sodium alginate/cellulose aerogel for the dye adsorption and oil-water separation

Huimin Li [a,b], Jingyi Huang [a], Chaoran Meng [a], Shen Shen [a,b], Hongbo Wang [a*], Jiajia Fu [a,b*]

[a] Jiangsu Engineering Technology Research Centre for Functional Textiles, Jiangnan University, No.1800 Lihu Avenue, Wuxi, P.R. China

[b] China National Textile and Apparel Council Key Laboratory of Natural Dyes, Soochow University, Suzhou 215123, China

Abstract

The wide application of polysaccharide-based aerogel is limited by its hydrophilicity. To solve this problem, sodium alginate/ sodium carboxymethyl cellulose (SA/CMC) with silica nanoparticles and methyl trimethoxysilane as hydrophobic modifiers was prepared in this study. The sodium alginate (SA) and sodium carboxymethyl cellulose (CMC) were selected because of their low cost and easy of combination with the other two materials. After the silane reagent modification, Ca^{2+} crosslinking, surface plasma treatment, thermochemical vapor deposition and freeze-drying methods, the aerogel get density of 0.080 g/cm^3, high porosity of 94%, three-dimensional porous structure with great adsorbed ability. This superhydrophobic SA/CMC aerogel exhibits excellent water stability, appropriate compressive strength and good adsorption capacity of cationic dye methylene blue (MB). And the adsorption process is analyzed by adsorption kinetics. Meanwhile, this aerogel gets great absorbency and efficiency towards varieties of organic solvents, which gives it great potential of being used in the field of oil-water separation, textile dye wastewater treatment, etc. Moreover, this aerogel is expected to be

* Corresponding author; e-mail: kathyfjj@126.com ; wxwanghb@163.com

recycled after washing.

Keywords

Polysaccharide-based aerogel; Hydrophobicity; Dye adsorption; Oil-water separation;

Introduction

With the development of the industrialization, organic water pollution (e.g., textile dye wastewater treatment, oil spill, etc) is becoming more and more serious, which caused serious problem to the ecological environment (Lee et al. 2017). Thus, developing novel materials for removing the organic pollutants out of water effectively is of great urgent. And aerogels showed great potential under this circumstances (Zhang et al. 2020). Aerogel is a sort of porous and light-weight materials widely used in the field of catalysis (Niu et al. 2020), adsorption and environmental clean-up (Zhang et al. 2017, Matias et al. 2015, Perdigoto et al. 2012, Guan et al. 2020, Adebajo et al. 2003), acoustic transducers (Long et al. 2021), energy storage devices (Long et al. 2008), thermal isolation (Zheng et al. 2020), flame retardant (Chen et al. 2016), chemical sensors (Plata et al. 2004), and biomedical and pharmaceutical applications (Smirnova et al. 2004, Ulker & Erkey 2014, Yan et al. 2020). Up to our knowledge, the potential application of the aerogel is strongly relied on the materials and microstructure. The microstructure can be controlled during the preparation process, including the sol-gel transition (gelation), network perfection (aging) and gel-aerogel transition (drying) (Zuo et al. 2015). The starting precursors, operating and provision requirements are the decisive factor in a sol-gel reaction of wet chemical synthesis approach to prepare aerogels. Moreover, the generation of the 3D porous network is the most determinant aspect of aerogel fabrication (Maleki 2016, Estella et al. 2007). Although the biodegradable polysaccharide-based aerogels showed great promise in the area of oil-water separation, they are extremely fragile and easy to collapse in water due to the hydrophilicity property of the materials (Fu &

Guo 2022, Alvarez-Lorenzo et al. 2013, Reches & Gazit 2003, Autissier et al. 2010, Benbettaieb et al. 2016). Therefore, the polysaccharide aerogel without hydrophobic modification, as adsorbent or catalyst, will seriously affect the adsorption effect or catalytic efficiency. It has practical significance to extend and promote the application of the eco-friendly polysaccharide aerogel by changing its hydrophilicity.

Alginate and cellulose, both natural polysaccharide that have shown great potential as the most important biocompatible and eco-friendly polymers in nature, which are rich in resources. The evaporation of absorbed water molecules often causes the structure of aerogel to collapse. There are limited its application due to poor mechanical properties and excellent hydrophilicity in the dye adsorption, oil-water separation and recyclability. On the one hand, sodium alginate (SA) can form a 3D network with a unique "egg-box" structure upon ionic crosslinking with divalent cations such as calcium, because the cations cause the G-units on neighboring polysaccharide chains to interact, corresponding to the gels stack that form the structure of the cross-linking network (Jing et al. 2022, Gao et al. 2021, Jeong et al. 2010). Meantime, cellulose derivative aerogels can be prepared by derivatization of cellulose and chemical crosslinking of crosslinking agent (Tan et al. 2001). Sodium carboxymethyl cellulose (CMC), as a solubility polysaccharide with biocompatibility and biodegradation, is a common derivates formed by the carboxymethylation of the hydroxyl group of cellulose (Lin et al. 2016). CMC can facilely and quickly cross linked with metal ions (such as Ca^{2+}, Mg^{2+}, Al^{3+} and Fe^{3+}) in non-toxic and eco-friendly reaction environment (Lin et al. 2016, Nie et al. 2004, Li et al. 2013, Nadagouda & Varma 2007). On the other hand, the bionic superhydrophobic materials, as a recent research hotspot, are mainly constructed according to the superhydrophobic lotus surface and typical "rose petal" effect in nature (Li et al. 2017). The constructed fabric surfaces with microtemplates for patterning, which are based on the morphology of particles coated on the textile fibre and exhibit an anti-wetting property. Moreover, the

65 superhydrophobic surfaces generally needs the introduction of surface roughness. The hydrophobic
66 interface with hierarchical cellular structure can be achieved by constructing rough micro and nano
67 texturing or introducing low surface energy substances (Li et al. 2017, Wang & Jiang 2007). Hereby, the
68 efficient way of superhydrophobic polysaccharide-based aerogel via silane reagent modification is the
69 most common preparation (Feng et al. 2015). Besides, plasma processing is a kind of modification
70 method with fast etching speed, high uniformity and low pollution in the processing method of
71 microscopic rough structure (Tsougeni et al. 2007). Moreover, the vapour deposition of hydrophobic
72 silanes on sponge-like ultra-porous nanocellulose aerogels can separate the mixed oil and water liquids
73 (Cervin et al. 2012). Xiao et al. developed a superhydrophobic and superelastic graphene oxide/nanofiber
74 aerogel (GNA) after chemical modification and crosslinking via vapor deposition of
75 hexadecyltrimethoxysilane to quickly separate oil-in-water emulsions with an extremely high flux (Xiao
76 et al. 2018). Yang et al. fabricated a robust and superhydrophobic sodium alginate/graphene oxide/silicon
77 oxide aerogel (SA/GO/SiO_2-M) by calcium ion cross-linking self-assembly and chemical vapor
78 deposition, which possesses high efficiency in the separation of surfactant-stabilized water-in-oil
79 emulsions with excellent reusability (Yang et al. 2021).

80 Herein, a superhydrophobic SA/CMC aerogel with silica nanoparticles was fabricated via silane
81 reagent modification, Ca^{2+} crosslinking, surface plasma treatment, thermochemical vapor deposition and
82 freeze-drying methods. The aerogel is explored the adsorption performance and oil-water separation
83 performance for cationic dye methylene blue (MB) and organic solvents. The effect of multi-step process
84 on hydrophobicity was studied in detail through the characterization of selective wettability,
85 adsorbability of various organic solvents, and oil-water separation capability. Meanwhile, the adsorption
86 process of cationic dye MB on the superhydrophobic SA/CMC aerogel was analyzed by the adsorption

kinetics analysis. This study shows that the superhydrophobic SA/CMC aerogel are a promising material in treating wastewater pollution from different fields.

2. Materials and methods

2.1 Materials

Sodium carboxymethyl cellulose (CMC, viscosity: 20 g/L solution, 300−800 mPa · s) and sodium alginate (SA, viscosity: 10 g/L solution, 20℃, ≥ 0.02 Pa · s) were obtained from Sinopharm Chemical Reagent Co., Ltd. (China). Silica (SiO_2) nanoparticles with diameter 15 ± 5 nm and the purity of 99.8 wt% was supplied by Shanghai Macklin Biochemical Co., Ltd. (China). Trimethoxymethylsilane (MTMS, purity ≥ 98 wt%), calcium chloride anhydrous ($CaCl_2$), hexane, anhydrous ethanol (AE) and other chemical reagents were also purchased from Sinopharm Chemical Reagent Co., Ltd. (China). Deionized water (DW) used in the experiments was obtained using an ULUPURE pure water/water system.

2.2 Preparation of the superhydrophobic SA/CMC aerogel

In our present study, we prepared the superhydrophobic SA/CMC aerogel via silane reagent modification, Ca^{2+} crosslinking, surface plasma treatment, thermochemical vapor deposition and freeze-drying methods. SA and CMC were dissolved into 2.0 wt % with optimal stock solutions volume ratios of SA/CMC (m/m) of 1/1 proceeding 2 h at 850 rpm under the condition of agitation at 30 ℃. By the way, the freeze-dried sample obtained at this time was distinguished as the SA/CMC aerogel. Briefly, a certain amount of silica nanoparticles (m(SA): m(CMC): m(SiO_2) =10:10:1) was added to the mixture and stirred at 850 rpm for 1 h, and 10 % of the volume fraction of MTMS was also added into the mixture and stirred at 850 rpm for 1 h. Then, the evenly dispersed mixture was sonicated for 30 min before freezing at -80 ℃ to remove large trapped air bubbles. After freeze-drying, the resulting aerogel was

immersed into impregnation solution (m ($CaCl_2$): m (AE): m (DW) = 2:80:20) for 12 h, and washed with an excess amount of DW and freeze-dried again. The obtained aerogel was surface modified by low-temperature plasma treatment in a condition of argon atmosphere for 10 min. Afterward, the aerogel was obtained in the simple reaction device of cup in cup with MTMS at 80 ℃ for 4 h. This device of cup in cup is mainly to prevent direct contact between aerogel sample and MTMS liquid. After fully reaction, the aerogel was placed in a vacuum drying oven with low pressure to remove the unreacted MTMS. Finally, the superhydrophobic SA/CMC aerogel was obtained (**Scheme 1**, **Support Information S1).**

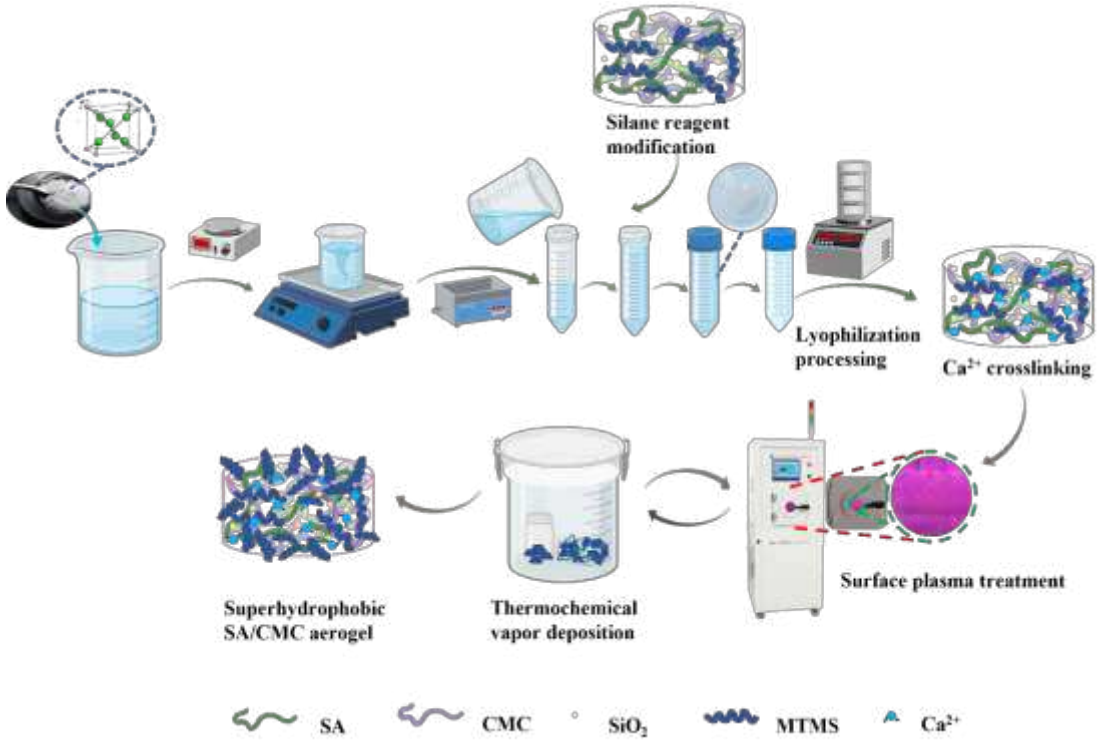

Scheme 1. Schematic illustration the treatment and possible hydrophobic modification mechanism of the superhydrophobic SA/CMC aerogel.

2.3 Physicochemical Characterizations of the superhydrophobic SA/CMC aerogel

The surface morphologies of samples were captured by scanning electron microscope (SEM SU1510, JPN). The molecular and crystallographic structures of samples were investigated by FT-IR spectrophotometer (Nicoletis10, USA) using KBr disk method in the range of 4,000–500 cm^{-1}. The

crystal-lographic structures of samples were characterized by X-ray diffraction diffractometer (XRD D2 PHASER, GER) with a CuKa radiation (k = 0.15405 nm) with a scanning rate of 2 min^{-1} at 40 kV and 40 mA. The un-treated linen fabric (s0) was also analyzed for comparison.

Measurement for the physical properties of the superhydrophobic SA/CMC aerogel

The thermal stabilities of samples were determined by thermo-gravimetric analyzer (TGA, Q500, USA) with a heating rate of 10 ℃ min-1 under N2 environment from 40 C to 800 ℃ as the test temperature range. Stress-strain curves were obtained by Universal Mechanical Materials Tester with loading speed of 10 mm·min^{-1} and 80 % of strain is the test end point. Each sample was tested three times to get the average value.

2.4 Density and porosity

The diameter and thickness of samples (circular shape) were measured separately. The density was calculated using the formula (1).

$$\rho = \frac{m}{V} \qquad (1)$$

where m and V are the weight and volume of samples, respectively.

The liquid displacement method was used to determine the porosity of samples. The samples (cube, 1 cm×1 cm×1 cm) were put into anhydrous ethanol (AE) to reach a saturation point. All tested samples were gently blotted with filter paper to remove the excess AE and to get the immediately weighed (W). The porosity was calculated using the formula (2).

$$P\ (\%) = \frac{(W - W_0)}{\rho_a V} \times 100\% \qquad (2)$$

where W_0 and W are the weight of samples before and after being immersed in AE, respectively; V is the sample volume before immersion and ρ_a is the density of alcohol.

2.5 Measurement of water stability for the superhydrophobic SA/CMC aerogel

The water contact angles (WCAs) were measured at room temperature and ambient relative humidity using a DSA25 contact angle analyzer connected to drop shape analysis software. The water contact angles for each sample were measured more than five times on the SA/CMC aerogel and the superhydrophobic SA/CMC aerogel. The water stability of the prepared aerogel in the water was also investigated (**Support Information S2)**.

2.6 Dye adsorption performance test

Methylene blue trihydrate ($C_{16}H_{18}ClN_3S{\cdot}3H_2O$) (Kannan & Sundaram 2001) was dissolved in various concentrations (0.6 mg/L 0.8 mg/L 1.0 mg/L 2.0 mg/L 4.0 mg/L), which were used as MB standard solutions of the concentration required by the experiment. DW was used as control group and measurement baseline. Then the standard concentration gradient of MB solution of samples was determined spectrophotometrically at 664 nm following the Bouguer-Beer-Lambert Law (Mayerhofer et al. 2020). The concentration of residual dye in different MB solution was measured after equal-weight samples reached the adsorption equilibrium in 50 mL centrifuge tube at 200 rpm. The removal percentage and adsorption value of MB were calculated using the formula (3)(4)(5).

$$R_e\ (\%) = \frac{C_0 - C_e}{C_0} \times 100\% \qquad (3)$$

$$Q_e = \frac{(C_0 - C_e)V_d \times N}{m_0} \qquad (4)$$

$$Q_t = \frac{(C_0 - C_t)V_d \times N}{m_0} \qquad (5)$$

where R_e (%), Q_e and Q_t (mg/g) are dye removal percentage, dye adsorption capacity at equilibrium and t moment, respectively; C_0、C_e and C_t (mg/L) are the dye concentration at initial, equilibrium and t moment, respectively; V_d (L) is the volume of the dye solution; m_f (g) is the initial mass of the aerogel; N is dilution ratio.

2.7 The adsorption kinetics of the superhydrophobic SA/CMC aerogel

167 The pseudo-second-order model and intra-particle diffusion can be used to explore the adsorption
168 rate and behavior of pollutants on aerogel for studying its adsorption kinetics (Vimonses et al. 2009, Ho
169 & McKay 1999). The pseudo-second-order model can be used to judge the adsorption properties of
170 aerogel, which were calculated using the formula (6).

171 $$\frac{t}{Q_t} = \frac{1}{K_2 Q_e{}^2} + \frac{t}{Q_e} \quad (6)$$

172 Where Q_e, Q_t (mg·g^{-1}) are the adsorption capacity at equilibrium and t moment, respectively. K_2 (mg·g^{-1}·min^{-1})
173 is the pseudo-second-order model rate constant and t (min) is adsorption time.

174 The adsorption rate of adsorbents on porous material is usually controlled by the transfer rate at the
175 solid-liquid interface or inside the particle. The intra-particle diffusion within the particle is often used
176 to evaluate the diffusion mechanism of the adsorption process, which were calculated using the formula
177 (7).

178 $$Q_t = K_{id} t^{1/2} + C_{id} \quad (7)$$

179 Where K_{id} (mg·g^{-1}·min$^{-1/2}$) is diffusion rate constant of the intra-particle diffusion. The larger the
180 diffusion rate constant is, the easier the adsorbent diffuses inside the adsorbent. C_{id} is a constant involving
181 the boundary molecular layer including thickness and boundary layer. A linear line with slope K_{id} and
182 intercept C_{id} can be obtained by drawing $t^{1/2}$ and Q_t. The adsorption process is controlled by a single rate
183 of intra-particle diffusion if the line passes through the origin. Otherwise, the adsorption process is
184 controlled by both intra-particle and interfacial diffusion (Kannan & Sundaram 2001).

185 **2.8 Adsorption performance test of simulated organic pollutants**

186 In order to test the adsorption performance of the superhydrophobic SA/CMC aerogel on organic
187 pollutants, such as hexane, chloroform, oil pumping, AE, toluene and paraffin liquid were selected as the
188 adsorbent of organic solvents. And the adsorption capacity and adsorption rate of prepared aerogel were

measured respectively to evaluate the adsorption performance of the prepared aerogel. Samples of the same weight were put into 35 mL of various organic solvents to reach adsorption equilibrium at room temperature, then removed from various organic solvents. All tested samples needed gently blotted with filter paper to remove the excess various organic solvents and got the immediately weighed. Each sample was tested three times to get the average value. The adsorption performance was calculated using the formula (8)(9).

$$M_{oil/org} = \frac{m_s - m_0}{m_0} \quad (8)$$

$$V_{oil/org} = \frac{\rho}{\rho_{oil/org}} \times \frac{m_s - m_0}{m_0} \quad (9)$$

where $M_{oil/org}$ (g/g) is mass adsorption capacity ratio; $V_{oil/org}$ (cm^3/cm^3) is the volume adsorption capacity ratio; m_s and m_0 (g) are the weight of samples before and after being immersed in various organic solvents; ρ and $\rho_{oil/org}$ (g/cm^3) are the density of aerogel and various organic solvents, respectively.

2.9 Oil-water separation experiment

Hexane and chloroform were selected as two kinds of oils and organic solvents with opposite density compared with water. Chloroform ($\rho_{chloroform} > \rho_{water}$) and hexane ($\rho_{hexane} < \rho_{water}$) were dyed red with sudan red G and DW blue with methylene blue. The oil-water separation performance of the superhydrophobic SA/CMC aerogel (circular shape, diameter: 15 mm ± 0.1mm, thickness: 3 mm ± 0.1mm) was quantitatively characterized by filtration with 10 mL syringe. Chloroform, hexane and DW were mixed at a 1:1 volume ratio to form 4 mL oil-water mixture, which poured into the 10 mL syringe containing aerogel. Meanwhile, the glass bottle was placed under the syringe hole as a liquid collection device to conduct oil-water separation test and observe the effect. The separation efficiency is characterized by the volume ratio or mass ratio of the liquid collected before and after separation. The separation efficiency is calculated by measuring the mass of the liquid before and after separation using

211 the formula (10):

212 $$\eta(\%) = \frac{m_b}{m_a} \times 100\% \qquad (10)$$

213 where η (%) is the separation efficiency; m_a and m_b (g) are the mass of oil before and after filtration,

214 respectively.

215 The oil-water separation flow rate of aerogel can be expressed by the fluid flux of aerogel (F), which

216 is an important index to measure the oil-water separation performance of aerogel and can be obtained by

217 the following formula (11):

218 $$F = \frac{V}{A} \times \Delta t \qquad (11)$$

219 Where F is the fluid flux of aerogel; V (mm^3) is the volume of filtrate collected after separation

220 experiment through aerogel; A (mm^2) is the effective filtration area of separation experiment; Δ t (s) is

221 the time required for the whole oil-water separation experiment to pass through the aerogel.

222 **3 Results and Discussion**

223 **3.1. Characterization of the superhydrophobic SA/CMC aerogel**

224 The morphology is a vital feature for various samples. **Fig.1** shows the microstructure of the

225 SA/CMC aerogel and the superhydrophobic SA/CMC aerogel. The surface of the SA/CMC aerogel is

226 smooth and flat, and the pore structure is not obvious and irregular with small cracks locally. After

227 hydrophobic modification, the morphological changes of the superhydrophobic SA/CMC aerogel are

228 obviously observed. The porous structure presents an increasingly pronounced pore in size of 20 μm with

229 rough surface.

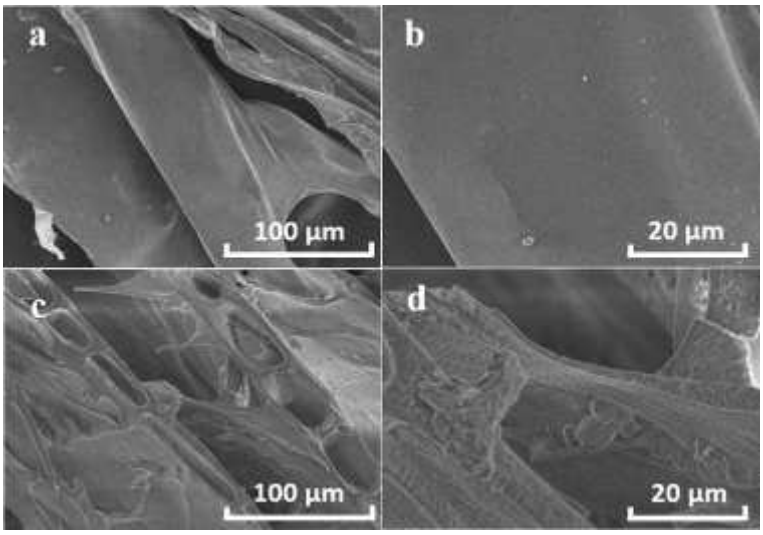

Fig. 1. Scanning electron microscope (SEM) images of **(a, b)** the SA/CMC aerogel and its high magnification, **(c, d)** the superhydrophobic SA/CMC aerogel and its high magnification.

The FIIR spectra of the SA/CMC aerogel and the superhydrophobic SA/CMC aerogel are compared in **Fig. 2**. The bands of SA at 1600 cm^{-1} are attributed to asymmetric stretching vibrations of COO^- (Jiao et al. 2016). The absorption peaks at 1600 cm^{-1} and 2920 cm^{-1} are found in all spectra, which are mainly ascribed to the carbonyl group (C=O), and the C-H bond on the molecular chain of SA and CMC, respectively. The characteristic peaks at 3350 cm^{-1} in all spectra are ascribed to O-H on SA and CMC. The superhydrophobic SA/CMC aerogel showed several new absorption peaks at 1269 and 768 cm^{-1} appeared due to Si-O and Si-O-Si bonds in silicane, respectively. The characteristic peaks at 2980 cm^{-1} corresponded to the vibrations of CH_3 bond (Robb et al. 2002) (Zhou et al. 2018, Zhou et al. 2015). In addition, C-O stretching vibration absorption peaks at 1100−1000 cm^{-1} are slightly strengthened, which is probably due to the coincidence of Si-O-Si absorption peaks. These indicate that MTMS successfully modified the superhydrophobic SA/CMC aerogel and formed covalent bond with hydroxyl group through dehydration condensation.

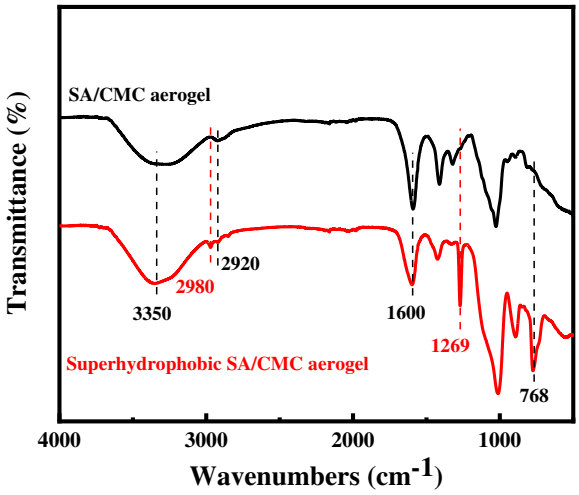

246

247 **Fig. 2.** FT-IR spectra of the SA/CMC aerogel and the superhydrophobic SA/CMC aerogel.

248

249 The crystalline structures of the SA/CMC aerogel and the superhydrophobic SA/CMC aerogel were
250 determined by X-ray diffraction patterns. Obviously, **Fig.** 3 exhibits the SA/CMC aerogel has the higher
251 crystallinity than the superhydrophobic SA/CMC aerogel. There are two distinct characteristic diffraction
252 peaks at 2θ =10.2° and 2θ =21.5° in the SA/CMC aerogel, while there is not obvious diffraction peak in
253 the superhydrophobic SA/CMC aerogel. The main reason is that the adding of SiO_2 nanoparticles and
254 trimethoxymethylsilane and subsequent hydrophobic modification disrupt the arrangement of polymer
255 crystals and form irregular and amorphous regions leading to the low crystallinity of superhydrophobic
256 SA/CMC aerogel (Abhari et al. 2017). It ensured the uniform mixing of them and prevented the
257 crystallization behavior of the SA/CMC aerogel. Thus the amorphous composite superhydrophobic
258 SA/CMC aerogel formed (Chang et al. 2009).

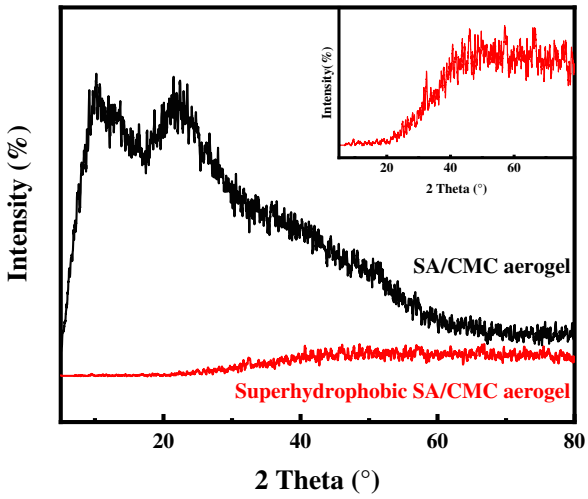

Fig. 3. X-ray diffraction pattern of the SA/CMC aerogel and the superhydrophobic SA/CMC aerogel.

3.2 The thermal stability of the superhydrophobic SA/CMC aerogel

The thermo-stabilities of the SA/CMC aerogel and the superhydrophobic SA/CMC aerogel were evaluated by the thermogravimetry analysis (TGA) and differential thermogravimetry (DTG). As shown in **Fig. 4**, the two kinds of aerogels exhibit four steps of active weight loss with elevating temperature. The rapid weight loss below 100 °C was attributed to the release of moisture from the aerogels. In the dehydration stage, the weight loss rate of the SA/CMC aerogel and the superhydrophobic SA/CMC aerogel reached about 19% and 13 %, respectively. The main reason is that the escape of adsorbed water on the surface and internal pores of aerogels during evaporation. It is speculated that the reason for the difference is that the internal and surface structures of the two kinds of aerogels are significantly different with pore sizes and adsorbed moisture content. On the other hand, the differences in hygroscopicity of aerogels are reflected the hydrophobic modification can significantly reduce the hygroscopicity of aerogel. In addition, the initial thermal decomposition temperature of aerogels ranges from 200℃ to 350℃. The polysaccharide base polymer network structure begins to depolymerize and the chain

structure breaks, resulting in a very significant weight loss region of aerogel at this stage (Abhari et al. 2017, Liang & Hirabayashi 1992). The mass loss rates of aerogel and hydrophobic aerogel were as high as 34% and 12%, respectively, which showed significant differences. Then, the aerogels slowly loses weight with the increase of temperature from 350℃ to 540℃, suggesting that the components in aerogels are further thermologically decomposed. Moreover, the weight loss rate of the superhydrophobic SA/CMC aerogel is always smaller than that of the SA/CMC aerogel. In addition, the temperature higher than 540℃ is the carbonization stage of aerogel. With the increase of temperature, the trend of weight loss rate curve of aerogels shows that polysaccharides and other components are completely thermal degraded to form carbon oxides, and finally become inorganic components. The initial decomposition temperature of the superhydrophobic SA/CMC aerogel increased from 250 °C of the SA/CMC aerogel to 270 °C, and the maximum decomposition temperature also increased from 269 °C of the SA/CMC aerogel to 326 °C. It indicated that the reduction in crystallinity after hydrophobic modification has little effect on the increase of the thermal stability of the superhydrophobic SA/CMC aerogel. Besides, Ca^{2+} crosslinking can form a 3D network with a unique “egg-box” structure upon ionic crosslinking. SA and CMC produce strong chemical bonds with MTMS and Ca^{2+} leading to a tighter and more solid structure. Thus, the relatively high thermal stability appeared in superhydrophobic SA/CMC aerogel.

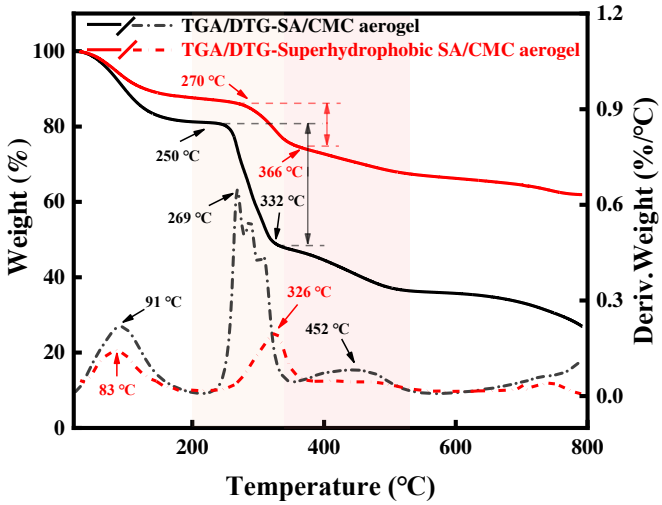

Fig. 4. Thermogravimetric analysis of the SA/CMC aerogel and the superhydrophobic SA/CMC aerogel about TGA curves and DTG curves.

3.3. Functionalities of the superhydrophobic SA/CMC aerogel

The porosities of the aerogels are decreasing with the increase of polysaccharide concentration in **Fig 5**a. This trend is contrary to the density of the aerogels curve. The porosities of the SA/CMC aerogel and the superhydrophobic SA/CMC aerogel are 97.64% and 94.16%, respectively. The densities of the SA/CMC aerogel and the superhydrophobic SA/CMC aerogel are 0.03129 and 0.0794 g/cm^3, respectively. **Fig 5**b indicating the superhydrophobic SA/CMC aerogel can stand on the top of flower stamens and dried flower because it's light enough.

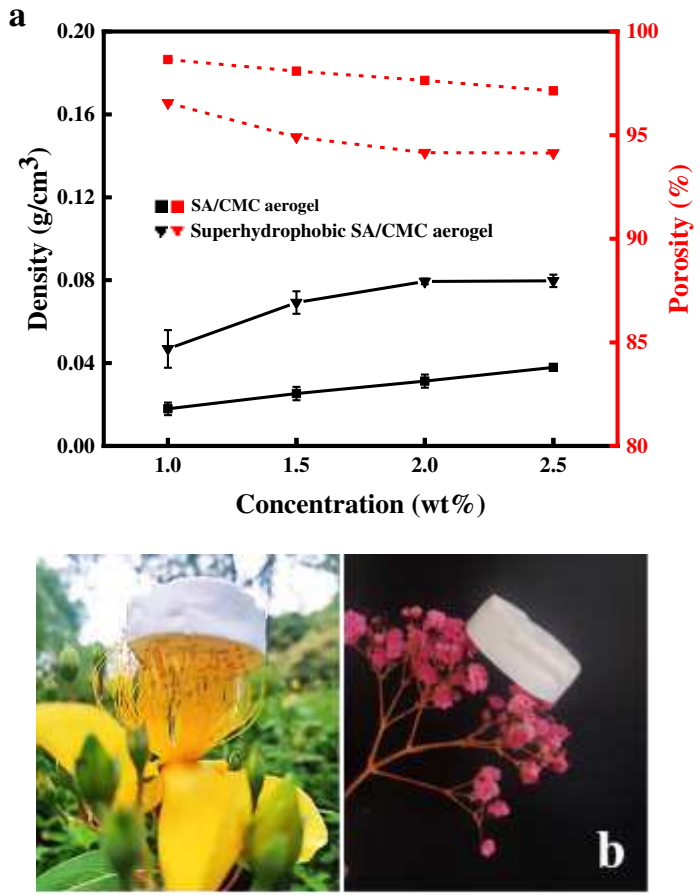

301

302

303 **Fig.5. (a)** Density and porosity of the SA/CMC aerogel and the superhydrophobic SA/CMC aerogel with

304 various concentration. Data are mean ± SD (n = 3); **(b)** Optical images indicating the superhydrophobic

305 SA/CMC aerogel can stand on the top of flower stamens and dried flower.

306

307 The perfect skeleton structure of aerogel can enhance its mechanical strength. Moreover, it plays an

308 important role in the process of oil adsorption and storage and oil-water separation. The compressive

309 stress-strain curves for the SA/CMC aerogel and the superhydrophobic SA/CMC aerogel are exhibited

310 in **Fig. 6**. The aerogels show different curves, indicating that the addition of SiO_2 nanoparticles and

311 hydrophobic modification influence the mechanical property of the SA/CMC aerogel. The

312 superhydrophobic SA/CMC aerogel could be compressed to more than 80% without mechanical failure

313 due to the flexibility of CMC and SA with Ca^{2+} crosslinking. The appropriate compressive stress would

be beneficial to the integrity maintenance in practical applications (Zhou et al. 2018).

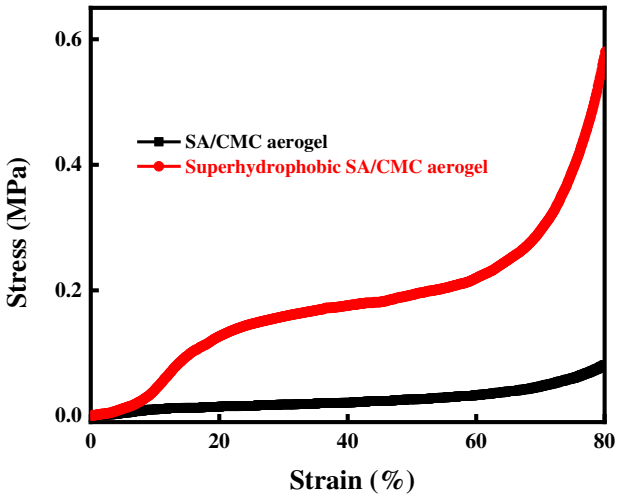

Fig.6. Compressive stress-strain curves of the SA/CMC aerogel and the superhydrophobic SA/CMC aerogel with strain of 80%.

The effect of each step in the hydrophobic modification process on the water stability of aerogels is shown in **Support Information S2**. Benefiting from the high surface roughness and polysaccharide matrix with porous structure, the superhydrophobic SA/CMC aerogel shows superhydrophobicity and superoleophilicity (Zhou et al. 2018). The WCAs for aerogels are exhibited in **Fig. 7**. As expected, the superhydrophobic SA/CMC aerogel was hydrophobic with a WCA of 161.5°, which could be ascribed to adding silica nanoparticles and successful silanizing modification. **Fig. 7**a exhibits the aerogel could leave the water droplets standing on its surface, while absorbing the chloroform droplet. As shown in **Fig. 7**b and **Support Information S3**, the water contact angles (WCAs, °) of SA/CMC aerogel with various concentration are 0°. All the hydrophobic modification steps promoted the hydrophobic properties of aerogels. A remarkable increase of WCA up to 161.5° was achieved with a series of hydrophobic modifications, demonstrating the superhydrophobicity of the obtained composite aerogels.

The hydrophobic properties of aerogels could be improved by increasing the concentration of polysaccharide and silane reagent in the same proportion. A preliminary hydrophobic modification process of silanization could be carried out in the sol-gel reaction process to improve the hydrophobicity of the SA/CMC aerogel. The obtained aerogel with preliminary hydrophobic modification using silane reagent has more stable structure and better performance after Ca^{2+} crosslinking. Further, surface plasma treatment prompts the hydroxyl functional groups on SA and CMC on the surface of the aerogel can be activated and exposed, which is conducive to thermochemical vapor deposition as the subsequent hydrophobic modification of silanization. Besides, the water droplet would return to its original shape immediately after leaving the surface of the aerogel. The resultant figures present that the superhydrophobic and superoleophilic SA/CMC aerogel with good hydrophobicity and low water adhesion ensured that the oil agent could permeate and move through it, which is good for the oil-water separation performance.

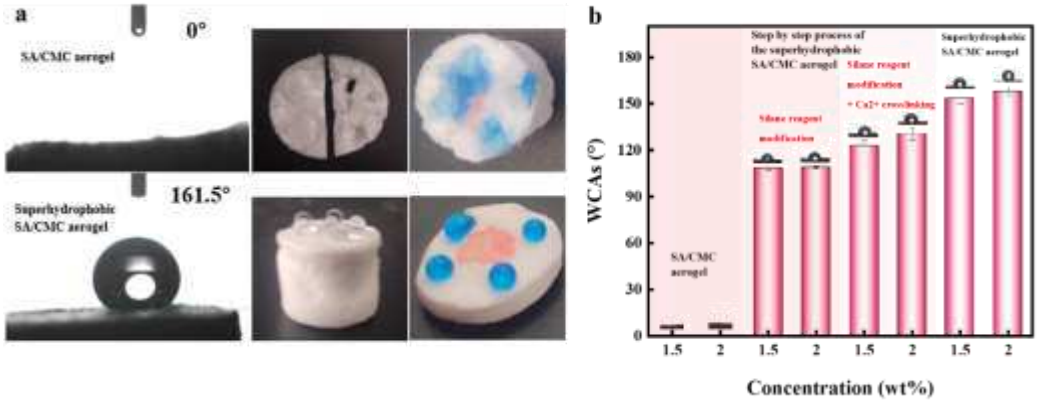

Fig.7. (a) Optical images of the process of water contacting the surface of two kinds of aerogels and water (blue) and chloroform (red) on the surface of them; **(b)**The water contact angles (WCAs, °) of the SA/CMC aerogel and the superhydrophobic SA/CMC aerogel with two kinds of polysaccharide concentrations in different processing stages when the water drops stabilized after falling (0.25 s). Data are mean ± SD (n = 3).

Methylene blue (MB, $C_{16}H_{18}ClN_3S$) is a widely used cationic dye, which can be selected as the target dye pollutant (Kannan & Sundaram 2001). The superhydrophobic SA/CMC aerogel could be used to adsorb the MB, and its equilibrium adsorption capacity increases with initial concentration. **Support Information S4** exhibits the correlation between the concentration of MB and its absorbance. As shown in **Fig. 8**, under the three different initial concentrations of MB, the equilibrium adsorption capacities of the superhydrophobic SA/CMC aerogel are 2.19 mg/g, 4.64 mg/g and 7.22 mg/g, and the dye removal percentage are 71.59 %, 75.79 % and 78.63 %, respectively. The main reason is the electrostatic attraction as the main force between aerogel and MB.

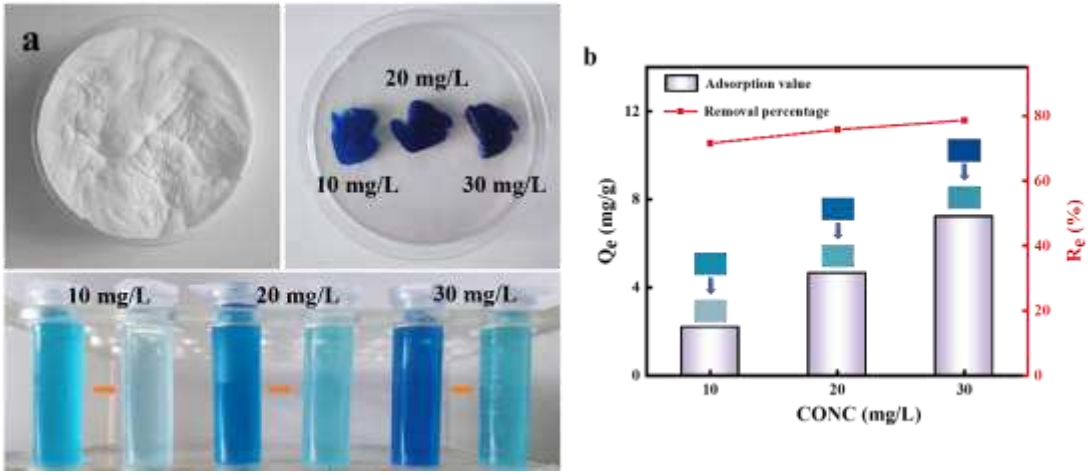

Fig.8. Optical images of the superhydrophobic SA/CMC aerogel and MB solution concentration changes **(a)** before and **(b, c)** after adsorption. **(d)** MB removal percentage and equilibrium adsorption capacity at different initial concentrations of MB.

According to the **Fig. 9** and **Table 1**, it can be seen the R_2^2 is greater than 0.999 that very close to 1, indicating that the experimental data are highly consistent with the curve fitted by the pseudo-second-order model. The value of Q_{ec2} is highly close to the Qee obtained from the actual experiment. Above all can show that the superhydrophobic SA/CMC aerogel of MB adsorption dynamics behavior conforms to

the pseudo-second-order model. The adsorption rate of MB by the superhydrophobic SA/CMC aerogel is linearly related to the mass of aerogel and the initial concentration of MB. The adsorption process is mainly chemical adsorption, which is closely related to the chemical composition of aerogel. The process of MB adsorption by the superhydrophobic SA/CMC aerogel could also be directly fitted to a continuous curve with linear relationship by the intra-particle diffusion. The straight line that passes through the origin and above it, indicating that the kinetic process of MB adsorption by aerogel is affected by both intra particle diffusion and boundary layer diffusion. As depicted in **Fig.9**c, the boundary molecular layer constant C_{id} as the intercept of the line is greater than 0, indicating that there is a rapid adsorption process in the process of MB adsorption, where the slope of the line represents the diffusion rate constant in the particle (Wu et al. 2009). Moreover, the higher the initial concentration of MB was, the lower the degree of linear fit of the model became. Therefore, the adsorption process can be further refined into three stages. The first stage is the surface adsorption stage within 30 min. The adsorption rate is the fastest and the intra-particle diffusion rate is the largest. The main reason is that the high initial concentration of MB and the high porosity of aerogel can quickly adsorb a large number of dye molecules in the solution. The second stage mainly occurred the adsorption rate gradually slows down in the 30-90 min period. The dye molecules gathered on the outer surface of aerogel would increase with time, and MB would diffuse in the small pores inside aerogel. The third stage occurs after 90 min of adsorption. There are fewer dye molecules in the solution. The active adsorption sites on aerogel surface decreased with the decrease of MB concentration. Therefore, the adsorption rate is the slowest and the diffusion rate in particles is the smallest at this stage. Finally, the adsorption equilibrium state will be reached.

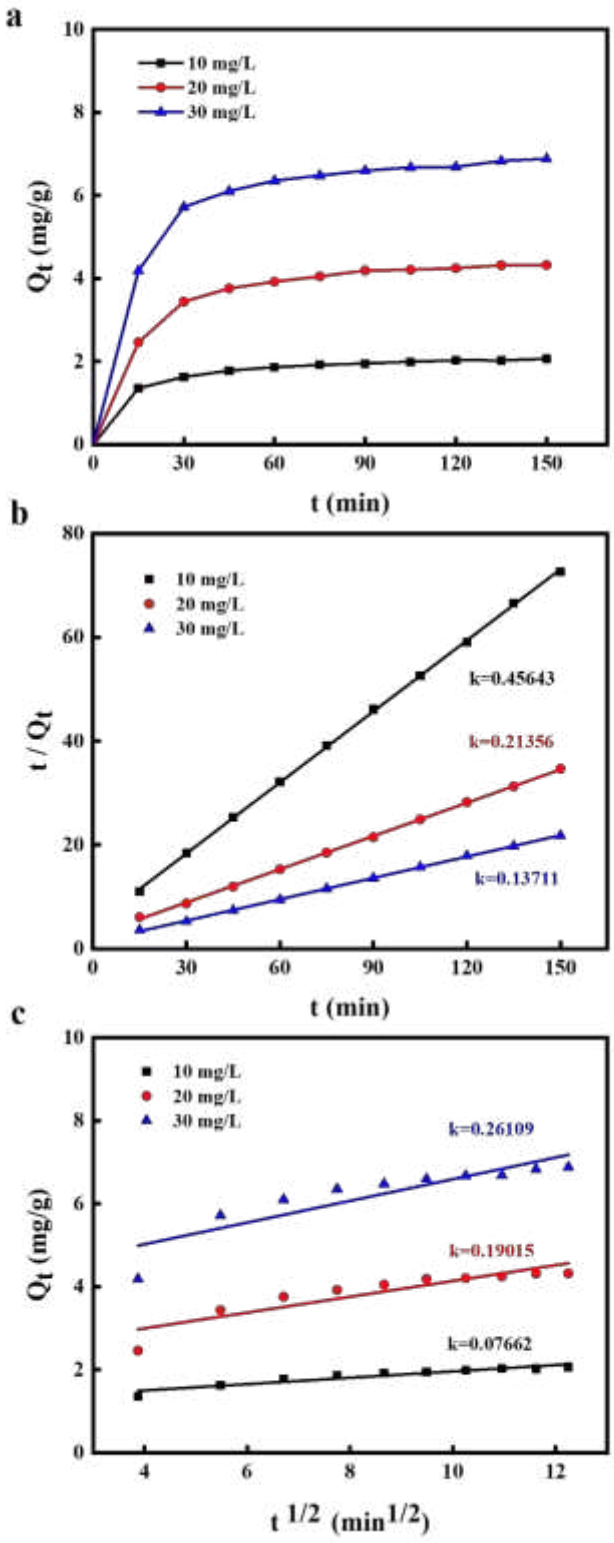

385

386 **Fig.9.** The influence of time on adsorption of MB with different initial concentrations by the

387 superhydrophobic SA/CMC aerogel and the fitting curves of adsorption kinetics **(a)**; fitting curve of

388 pseudo-second-order model **(b)**; fitting curve of intra-particle diffusion **(c)**.

Table 1. The adsorption kinetics parameters of the superhydrophobic SA/CMC aerogel for MB solutions with different initial concentrations

Kinetic model	C_0（mg/L）	K_2 (g/mg min)	Q_{ec2} (mg/g)	R_2^2
Pseudo-second-order	10	0.044649	2.190916	0.99977
	20	0.018212	4.682525	0.99963
	30	0.014491	7.293414	0.99959
Kinetic model	C_0（mg/L）	K_{id} (mg/g $min^{1/2}$)	C_{id} (mg/g)	R_3^2
Intra-particle diffusion	10	0.07662	1.19477	0.9054
	20	0.19015	2.23771	0.82331
	30	0.26109	3.97997	0.76405

The superhydrophobic SA/CMC aerogel is an ideal candidate for the sorption of organic pollutants due to its high porosity, compressive stability and hydrophobicity. The superhydrophobic SA/CMC aerogel has a certain weight and volume adsorption capacity for various oils and organic solvents are 6–12 g/g and 65%–80% in **Fig. 10**. It exhibits the oil droplet could be absorbed by the aerogel immediately when it contacted the aerogel surface. The superhydrophobic SA/CMC aerogel preferentially adsorbs to a layer of oils and organic solvents dyed red in the oil-water mixture, such as paraffin liquid**,** chloroform and hexane. In particular, chloroform has the best effect in the selective competitive adsorption process of the superhydrophobic SA/CMC aerogel in **Support Information S5**. Chloroform ($\rho_{chloroform} > \rho_{water}$, red) and hexane ($\rho_{hexane} < \rho_{water}$, red) were selected as two kinds of oils and organic solvents with opposite density compared with water (blue). In order to further demonstrate the absorbing capability of the superhydrophobic SA/CMC aerogel in oil-water separation, various kinds of

403 organic solvents (e.g., chloroform and hexane etc.) were tested by a simple device in **Fig.11**. The oil/water
404 mixture can be separated by gravity. The organic solvents could slowly permeate the aerogel and the
405 water is remains on top of the aerogel in the syringe. The separation efficiency of chloroform is 58.27%
406 and the fluid flux of oil-water separation is 74.66 mm·s. The aerogel will form an oil layer in the lower
407 layer because it has a certain adsorption effect on the oil, which prevents the further penetration of water
408 to successfully realize the separation of the oil-water mixture. Moreover, the superhydrophobic SA/CMC
409 aerogel has a good separation effect on oil-water mixture retaining original structure after adsorption.
410 However, the separation effect of this filtration method is not good for oil with density less than water
411 (**Fig.11**b). The main reason is that the oil contacted with the aerogel can percolate down to be collected
412 in the bottle. But the oil that has been blocked by the water layer from contacting the aerogel eventually
413 unable to be filtered by gravity when the oil-water mixture is poured. The superhydrophobic SA/CMC
414 aerogel after adsorbing organic liquids could be recycled by mechanically squeezing out oils or drying
415 absorbed samples at above the boiling point, which avoids the pollution and realizes the recyclability of
416 organic solvents further.
417

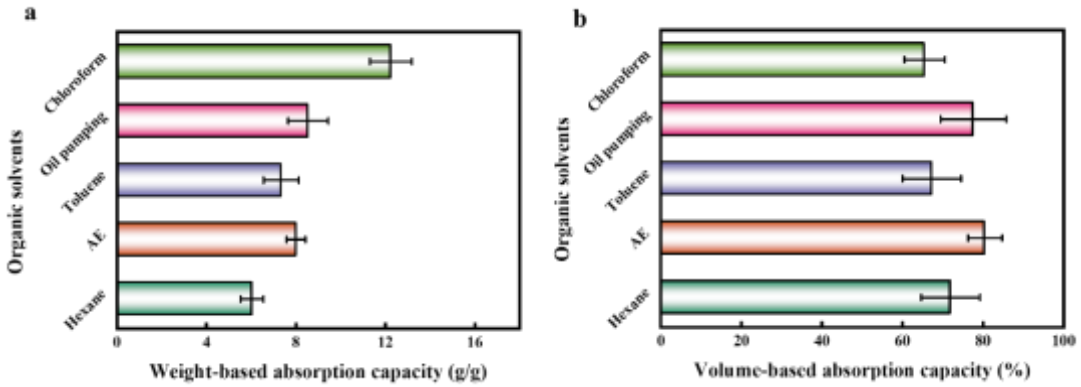

418

419 **Fig.10. (a)** Mass and **(b)** volumetric adsorption capacity of the superhydrophobic SA/CMC aerogel for
420 different oils and organic solvents ($\rho_{chloroform}$=1.484 g/cm^3, $\rho_{oil\ pumping}$ =0.874 g/cm^3, $\rho_{toluene}$ =0.866 g/cm^3,

421 ρ_{AE}=0.7893 g/cm^3, ρ_{hexane} =0.6594 g/cm^3).

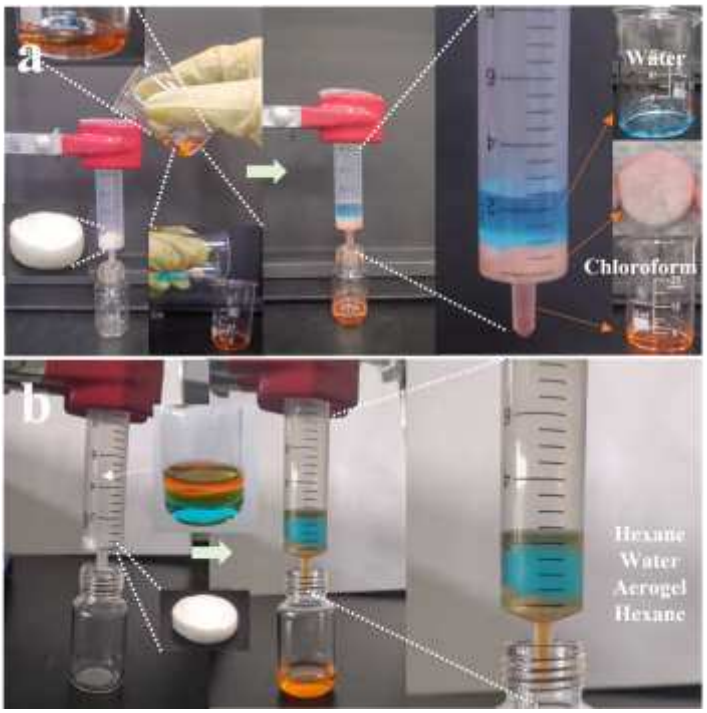

422

423 **Fig.11 (a, b)** Schematic diagram of oil-water mixture separation process.

424 **Table 2.** Separation effect of the superhydrophobic SA/CMC aerogel for chloroform /water mixture

Test	m_a/g	m_b/g	V/mm^3	A/mm^2	Δ t/s	η/%	F
1	2.9832	1.8545	1243.296	176.7146	10.03	62.16	70.57
2	2.9832	1.5304	1026.012	176.7146	12.61	51.30	73.21
3	2.9832	1.8302	1227.005	176.7146	11.55	61.35	80.20
Average	2.9832	1.7384	1165.438	176.7146	11.40	58.27	74.66

425

426 **4 Conclusion**

427 In this study, the superhydrophobic SA/CMC aerogel was successfully fabricated and demonstrated

428 the feasibility of an effective absorbent for targeting dye methylene blue (MB) and organic pollutants.

429 The advantages of aerogel also include a green preparation environment, and a mild modification method,

including silane reagent modification, Ca^{2+} crosslinking, surface plasma treatment, thermochemical vapor deposition and freeze-drying methods. The obtained aerogel represented superior physical features, including low density, high porosity, mechanical stability, superhydrophobicity, water stability and stable adsorption capacity for dyes and organic solvents. Furthermore, it is found that the initial MB concentration significantly affects the absorption capability of the aerogel. The pseudo-second-order model and intra-particle diffusion are applied to describe and validate the MB absorption behavior of the aerogel. Moreover, it could separate oil-water mixture without external pressure for various organic solvents. Consequently, the superhydrophobic SA/CMC aerogel offers a great feasibility for various applications in the fields of environment remediation, organic solvents purification and removal of organic liquids from waterbody etc.

Declarations

Conflict of interest

The authors declare that they have no known competing financial interests or personal relationships that could have appeared to influence the work reported in this paper.

Funding / Acknowledgments

We gratefully acknowledge the Support by the Opening Project of China National Textile and Apparel Council Key Laboratory of Natural Dyes, Soochow University (No.SDHY2122), the National Natural Science Foundation of China (No.31470509) and Jiangsu Natural Science Foundation for General project (BK20191199).

Author Contribution

CRediT authorship contribution statement

Huiming Li: Conceptualization, Investigation, Data curation, Writing - original draft. Jingyi Huang: materials preparation. Chaoran Meng and Shen Shen: review & editing. Hongbo Wang and Jiajia Fu: review & editing; Supervision & Funding acquisition. All authors reviewed the manuscript.

Ethics approval and consent to participate

Not applicable

Consent for publication

All authors believe that the findings of this study are relevant to the scope of your journal and will be of interest to its readership.

Availability of data and materials

The results/data/figures in this manuscript have not been published elsewhere, nor are they under consideration (from all authors) by another publisher.

Authors' information (optional)

Huimin Li

Jiangnan University

1800 Lihu Avenue, Wuxi 214122, China

Tel: 0086-15764233420

Email Address: 7200707007@stu.jiangnan.edu.cn

Jingyi Huang

Jiangnan University

1800 Lihu Avenue, Wuxi 214122, China

Email Address: hjy364570266@163.com

Chaoran Meng

Jiangnan University

1800 Lihu Avenue, Wuxi 214122, China

Email Address: 8202101470@jiangnan.edu.cn

Shen shen

Jiangnan University

1800 Lihu Avenue, Wuxi 214122, China

Email Address: 7170707009@stu.jiangnan.edu.cn

Hongbo Wang

Jiangnan University

1800 Lihu Avenue, Wuxi 214122, China

Email Address: wxwanghb@163.com

Jiajia Fu

Jiangnan University

1800 Lihu Avenue, Wuxi 214122, China

Email Address: kathyfjj@126.com

493 **References**

494 C. H. Lee, B. Tiwari, D. Zhang, Y. K. Yap (2017) Water purification: oil–water separation by
495 nanotechnology and environmental concerns. Environ Sci-Nano 4: 514-525.
496 https://doi.org/10.1039/c6en00505e

497 N. Zhang, Y. F. Qi, Y. N. Zhang, J. L. Luo, P. Cui, W. Jiang (2020) A Review on Oil/Water Mixture
498 Separation Material. Ind Eng Chem Res 59: 14546-14568.

499 T. T. Niu, B. Zhou, Z. H. Zhang, X. J. Ji, J. M. Yang, Y. H. Xie, . . . A. Du (2020) Low-Temperature
500 Synthesis of Monolithic Titanium Carbide/Carbon Composite Aerogel. Nanomaterials 10.
501 https://doi.org/10.3390/nano10122527

502 C. Z. Zhang, C. Dai, H. Q. Zhang, S. T. Peng, X. Wei, Y. D. Hu (2017) Regeneration of mesoporous silica
503 aerogel for hydrocarbon adsorption and recovery. Mar Pollut Bull 122: 129-138.
504 https://doi.org/10.1016/j.marpolbul.2017.06.036

505 T. Matias, J. Marques, M. J. Quina, L. Gando-Ferreira, A. J. M. Valente, A. Portugal, L. Duraes (2015)
506 Silica-based aerogels as adsorbents for phenol-derivative compounds. Colloid Surface 480: 260-269.
507 https://doi.org/10.1016/j.colsurfa.2015.01.074

508 M. L. N. Perdigoto, R. C. Martins, N. Rocha, M. J. Quina, L. Gando-Ferreira, R. Patricio, L. Duraes
509 (2012) Application of hydrophobic silica based aerogels and xerogels for removal of toxic organic
510 compounds from aqueous solutions. J Colloid Interface Sci 380: 134-140.
511 https://doi.org/10.1016/j.jcis.2012.04.062

512 Y. Guan, J. Rao, Y. L. Wu, H. Gao, S. Q. Liu, G. G. Chen, F. Peng (2020) Hemicelluloses-based magnetic
513 aerogel as an efficient adsorbent for Congo red. Int J Biol Macromol 155: 369-375.
514 https://doi.org/10.1016/j.ijbiomac.2020.03.231

M. O. Adebajo, R. L. Frost, J. T. Kloprogge, O. Carmody, S. Kokot (2003) Porous materials for oil spill cleanup: A review of synthesis and absorbing properties. J Porous Mat 10: 159-170. https://doi.org/10.1023/A:1027484117065

X. Long, X. B. Wei, Y. H. Qiu, M. Jiang, Z. Chen, Y. C. Song, . . . J. X. Liao (2021) Lead zirconate titanate aerogel piezoelectric composite designed with a biomimetic shell structure for underwater acoustic transducers. Chem Commun 57: 9764-9767. https://doi.org/10.1039/d1cc03037j

J. W. Long, A. E. Fischer, T. M. McEvoy, M. E. Bourg, J. C. Lytle, D. R. Rolison (2008) PMSE 430-Self-limiting electropolymerization en route to ultrathin, conformal polymer coatings for energy-storage applications. Abstracts of Papers of the American Chemical Society 236.

Q. Y. Zheng, Y. Tian, F. Y. Ye, Y. Zhou, G. H. Zhao (2020) Fabrication and application of starch-based aerogel: Technical strategies. Trends Food Sci Tech 99: 608-620. https://doi.org/10.1016/j.tifs.2020.03.038

H. B. Chen, P. Shen, M. J. Chen, H. B. Zhao, D. A. Schiraldi (2016) Highly Efficient Flame Retardant Polyurethane Foam with Alginate/Clay Aerogel Coating. Acs Appl Mater Inter 8: 32557-32564. https://doi.org/10.1021/acsami.6b11659

D. L. Plata, Y. J. Briones, R. L. Wolfe, M. K. Carroll, S. D. Bakrania, S. G. Mandel, A. M. Anderson (2004) Aerogel-platform optical sensors for oxygen gas. J Non-Cryst Solids 350: 326-335. https://doi.org/10.1016/j.jnoncrysol.2004.06.046

I. Smirnova, S. Suttiruengwong, W. Arlt (2004) Feasibility study of hydrophilic and hydrophobic silica aerogels as drug delivery systems. J Non-Cryst Solids 350: 54-60. https://doi.org/10.1016/j.jnoncrysol.2004.06.031

Z. Ulker, C. Erkey (2014) An emerging platform for drug delivery: Aerogel based systems. J Control

537 Release 177: 51-63. https://doi.org/10.1016/j.jconrel.2013.12.033

538 G. H. Yan, B. L. Chen, X. H. Zeng, Y. Sun, X. Tang, L. Lin (2020) Recent advances on sustainable
539 cellulosic materials for pharmaceutical carrier applications. Carbohyd Polym 244.
540 https://doi.org/10.1016/j.carbpol.2020.116492

541 L. Z. Zuo, Y. F. Zhang, L. S. Zhang, Y. E. Miao, W. Fan, T. X. Liu (2015) Polymer/Carbon-Based Hybrid
542 Aerogels: Preparation, Properties and Applications. Materials 8: 6806-6848.
543 https://doi.org/10.3390/ma8105343

544 H. Maleki (2016) Recent advances in aerogels for environmental remediation applications: A review.
545 Chem Eng J 300: 98-118. https://doi.org/10.1016/j.cej.2016.04.098

546 J. Estella, J. C. Echeverria, M. Laguna, J. J. Garrido (2007) Effects of aging and drying conditions on the
547 structural and textural properties of silica gels. Micropor Mesopor Mat 102: 274-282.
548 https://doi.org/10.1016/j.micromeso.2007.01.007

549 Y. Fu, Z. Guo (2022) Natural polysaccharide-based aerogels and their applications in oil–water
550 separations: a review. J Mater Chem A 10: 8129-8158. https://doi.org/10.1039/d2ta00708h

551 C. Alvarez-Lorenzo, B. Blanco-Fernandez, A. M. Puga, A. Concheiro (2013) Crosslinked ionic
552 polysaccharides for stimuli-sensitive drug delivery. Adv Drug Deliver Rev 65: 1148-1171.
553 https://doi.org/10.1016/j.addr.2013.04.016

554 M. Reches, E. Gazit (2003) Casting metal nanowires within discrete self-assembled peptide nanotubes.
555 Science 300: 625-627. https://doi.org/10.1126/science.1082387

556 A. Autissier, C. Le Visage, C. Pouzet, F. Chaubet, D. Letourneur (2010) Fabrication of porous
557 polysaccharide-based scaffolds using a combined freeze-drying/cross-linking process. Acta Biomater 6:
558 3640-8. https://doi.org/10.1016/j.actbio.2010.03.004

559 N. Benbettaieb, J. P. Gay, T. Karbowiak, F. Debeaufort (2016) Tuning the Functional Properties of
560 Polysaccharide-Protein Bio-Based Edible Films by Chemical, Enzymatic, and Physical Cross-Linking.
561 Compr Rev Food Sci F 15: 739-752. https://doi.org/10.1111/1541-4337.12210
562 H. J. Jing, X. Huang, X. J. Du, L. Mo, C. Y. Ma, H. X. Wang (2022) Facile synthesis of pH-responsive
563 sodium alginate/carboxymethyl chitosan hydrogel beads promoted by hydrogen bond. Carbohyd Polym
564 278. https://doi.org/10.1016/j.carbpol.2021.118993
565 C. Gao, X. L. Wang, Q. D. An, Z. Y. Xiao, S. R. Zhai (2021) Synergistic preparation of modified alginate
566 aerogel with melamine/chitosan for efficiently selective adsorption of lead ions. Carbohyd Polym 256.
567 https://doi.org/10.1016/j.carbpol.2020.117564
568 S. I. Jeong, M. D. Krebs, C. A. Bonino, S. A. Khan, E. Alsberg (2010) Electrospun Alginate Nanofibers
569 with Controlled Cell Adhesion for Tissue Engineering. Macromol Biosci 10: 934-943.
570 https://doi.org/10.1002/mabi.201000046
571 C. B. Tan, B. M. Fung, J. K. Newman, C. Vu (2001) Organic aerogels with very high impact strength.
572 Adv Mater 13: 644-646. https://doi.org/10.1002/1521-4095(200105)13:9<644::AID-
573 ADMA644>3.0.CO;2-#
574 R. J. Lin, A. Li, L. B. Lu, Y. Cao (2016) Preparation of bulk sodium carboxymethyl cellulose aerogels
575 with tunable morphology (vol 118, pg 126, 2015). Carbohyd Polym 151: 1278-1278.
576 https://doi.org/10.1016/j.carbpol.2016.05.071
577 H. R. Nie, M. Z. Liu, F. L. Zhan, M. Y. Guo (2004) Factors on the preparation of carboxymethylcellulose
578 hydrogel and its degradation behavior in soil. Carbohyd Polym 58: 185-189.
579 https://doi.org/10.1016/j.carbpol.2004.06.035
580 L. Li, S. L. Xiang, S. Q. Cao, J. Y. Zhang, G. F. Ouyang, L. P. Chen, C. Y. Su (2013) A synthetic route to

581 ultralight hierarchically micro/mesoporous Al(III)-carboxylate metal-organic aerogels. Nat Commun 4.
582 https://doi.org/10.1038/ncomms2757
583 M. N. Nadagouda, R. S. Varma (2007) Synthesis of thermally stable carboxymethyl cellulose/metal
584 biodegradable nanocomposites for potential biological applications. Biomacromolecules 8: 2762-2767.
585 https://doi.org/10.1021/bm700446p
586 S. H. Li, J. Y. Huang, Z. Chen, G. Q. Chen, Y. K. Lai (2017) A review on special wettability textiles:
587 theoretical models, fabrication technologies and multifunctional applications. J Mater Chem A 5: 31-55.
588 https://doi.org/10.1039/c6ta07984a
589 S. Wang, L. Jiang (2007) Definition of superhydrophobic states. Adv Mater 19: 3423-3424.
590 https://doi.org/10.1002/adma.200700934
591 J. D. Feng, S. T. Nguyen, Z. Fan, H. M. Duong (2015) Advanced fabrication and oil absorption properties
592 of super-hydrophobic recycled cellulose aerogels. Chem Eng J 270: 168-175.
593 https://doi.org/10.1016/j.cej.2015.02.034
594 K. Tsougeni, A. Tserepi, G. Boulousis, V. Constantoudis, E. Gogolides (2007) Control of nanotexture and
595 wetting properties of polydimethylsiloxane from very hydrophobic to super-hydrophobic by plasma
596 processing. Plasma Processes Polym 4: 398-405. https://doi.org/10.1002/ppap.200600185
597 N. T. Cervin, C. Aulin, P. T. Larsson, L. Wagberg (2012) Ultra porous nanocellulose aerogels as
598 separation medium for mixtures of oil/water liquids. Cellulose 19: 401-410.
599 https://doi.org/10.1007/s10570-011-9629-5
600 J. L. Xiao, W. Y. Lv, Y. H. Song, Q. Zheng (2018) Graphene/nanofiber aerogels: Performance regulation
601 towards multiple applications in dye adsorption and oil/water separation. Chem Eng J 338: 202-210.
602 https://doi.org/10.1016/j.cej.2017.12.156

603 Y. S. Yang, X. P. Chen, Y. M. Li, Z. C. Yin, M. T. Bao (2021) Construction of a Superhydrophobic Sodium
604 Alginate Aerogel for Efficient Oil Absorption and Emulsion Separation. Langmuir 37: 882-893.
605 https://doi.org/10.1021/acs.langmuir.0c03229
606 N. Kannan, M. M. Sundaram (2001) Kinetics and mechanism of removal of methylene blue by adsorption
607 on various carbons - a comparative study. Dyes Pigments 51: 25-40. https://doi.org/10.1016/S0143-
608 7208(01)00056-0
609 T. G. Mayerhofer, S. Pahlow, J. Popp (2020) The Bouguer-Beer-Lambert Law: Shining Light on the
610 Obscure. Chemphyschem 21: 2029-2046. https://doi.org/10.1002/cphc.202000464
611 V. Vimonses, S. M. Lei, B. Jin, C. W. K. Chowd, C. Saint (2009) Kinetic study and equilibrium isotherm
612 analysis of Congo Red adsorption by clay materials. Chem Eng J 148: 354-364.
613 https://doi.org/10.1016/j.cej.2008.09.009
614 Y. S. Ho, G. McKay (1999) Pseudo-second order model for sorption processes. Process Biochem 34:
615 451-465. https://doi.org/10.1016/S0032-9592(98)00112-5
616 C. Jiao, J. Xiong, J. Tao, S. Xu, D. Zhang, H. Lin, Y. Chen (2016) Sodium alginate/graphene oxide aerogel
617 with enhanced strength-toughness and its heavy metal adsorption study. Int J Biol Macromol 83: 133-41.
618 https://doi.org/10.1016/j.ijbiomac.2015.11.061
619 C. S. Robb, S. E. Geldart, J. A. Seelenbinder, P. R. Brown (2002) Analysis of green tea constituents by
620 HPLC-FTIR. J Liq Chromatogr R T 25: 787-801. https://doi.org/10.1081/Jlc-120003036
621 S. K. Zhou, T. T. You, X. M. Zhang, F. Xu (2018) Superhydrophobic Cellulose Nanofiber-Assembled
622 Aerogels for Highly Efficient Water-in-Oil Emulsions Separation. Acs Appl Nano Mater 1: 2095-2103.
623 https://doi.org/10.1021/acsanm.8b00079
624 S. K. Zhou, M. Wang, X. Chen, F. Xu (2015) Facile Template Synthesis of Microfibrillated

625 Cellulose/Polypyrrole/Silver Nanoparticles Hybrid Aerogels with Electrical Conductive and Pressure
626 Responsive Properties. Acs Sustain Chem Eng 3: 3346-3354.
627 https://doi.org/10.1021/acssuschemeng.5b01020
628 N. Abhari, A. Madadlou, A. Dini (2017) Structure of starch aerogel as affected by crosslinking and
629 feasibility assessment of the aerogel for an anti-fungal volatile release. Food Chem. 221: 147-152.
630 https://doi.org/10.1016/j.foodchem.2016.10.072
631 C. Y. Chang, B. Duan, L. N. Zhang (2009) Fabrication and characterization of novel macroporous
632 cellulose-alginate hydrogels. Polymer 50: 5467-5473. https://doi.org/10.1016/j.polymer.2009.06.001
633 C. X. Liang, K. Hirabayashi (1992) Improvements of the Physical-Properties of Fibroin Membranes with
634 Sodium Alginate. J Appl Polym Sci 45: 1937-1943. https://doi.org/10.1002/app.1992.070451108
635 F. C. Wu, R. L. Tseng, R. S. Juang (2009) Initial behavior of intraparticle diffusion model used in the
636 description of adsorption kinetics. Chem Eng J 153: 1-8. https://doi.org/10.1016/j.cej.2009.04.042
637

Supplementary Files

This is a list of supplementary files associated with this preprint. Click to download.

- SupportInformation.docx
- Graphicabstract.tif